

Anisotropic-dielectric-loaded corrugated guide

K.C.C.O.Senhorini, J.R.Descardecı,

*Department of Electrical Engineering, Federal University of Tocantins, UFT. Palmas, Brazil,
kathy@uft.edu.br, ricardo@uft.edu.br*

J.R.Bergmann

Department of Electrical Engineering PUC-RJ, Bergmann@cetuc.puc-rio.br

Abstract— In this paper, the boundary condition characteristic equation of the anisotropic-dielectric-loaded corrugated guide are developed. Dispersion curves of hybrid modes generated by the characteristic equation are presented and discussed. This paper also presents a technique to reduce the relative permittivity and create uniaxial anisotropy from isotropic homogeneous dielectric.

Index Terms— Antennas; Microwaves; Waveguides.

I. INTRODUCTION

Advances in satellite communication have increased the need for study of new satellite antennas with low cross polarization, high efficiency, low side lobes, low weight and wide operation frequency. This is because the needs of more stringent requirements for frequency reuse in order to increase the capacity in the satellite bands, launching costs and advances in technologies of others communication system devices. Normally, the feed element plays an important part in the overall characteristic of the earth-station satellite communication system [1-4]. This paper presents a new feed element configuration that can be used alone or in array systems. It is an anisotropic-dielectric-loaded corrugated guide. This new feed element is analyzed, and the characteristic equation for its propagating modes is presented. A technique is also presented to improve mechanical and homogeneity characteristics for the dielectric rod used. This technique reduces the permittivity of a homogeneous material so that return loss can be minimized avoiding the need of foam dielectric materials. This technique also creates a uniaxial anisotropy effect in the material, and this effect is analyzed by propagation mode dispersion curves. The HE₁₁ balanced hybrid mode is supported and it is expected low cross polarization and side lobes in a wide operation band. The feed geometry proposed in this paper makes possible a permittivity transition in the axial direction for optimal return loss. The uniaxial anisotropy can also be a parameter to improve the mode propagation characteristics, especially for the HE₁₁ balanced hybrid mode [3].

II. THEORY

A. Geometry of the problem

Fig 1 shows the anisotropic-dielectric-loaded corrugated guide. The anisotropic dielectric has optical

axis in the z-direction. r_1 is the dielectric rod radius, r_0 is the corrugated guide radius (without corrugations) and r_2 is r_0 plus corrugation depth.

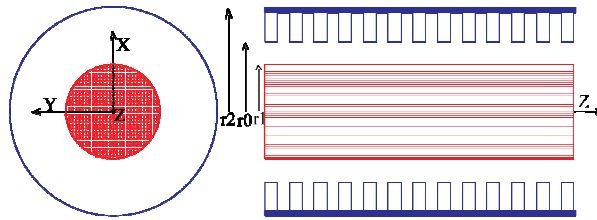


Fig. 1. Geometry of Anisotropic-dielectric-loaded corrugated guide.

B. Suggested technique to produce uniaxial anisotropy

It is suggested to produce anisotropy in the dielectric rod by perforating the dielectric in the axial direction (z-direction). The dielectric can be a PTFE (Polytetrafluoroethylene is a synthetic fluoropolymer of tetrafluoroethylene. It is most well known by the DuPont brand name Teflon) type material with a very good homogeneity. The idea is to achieve a more homogeneous and structurally strong material than the dielectric foam. The values of permittivity in the transversal (x and y-directions) and axial direction are given by the equations [5]:

$$\bar{\bar{\epsilon}} = \epsilon_0 \begin{pmatrix} \epsilon_t & 0 & 0 \\ 0 & \epsilon_t & 0 \\ 0 & 0 & \epsilon_z \end{pmatrix} = \epsilon_0 \bar{\bar{\epsilon}}_r \tag{1}$$

where:

$$\begin{cases} \epsilon_t = \epsilon_r (2 + C(\epsilon_r - 1)) / (2\epsilon_r - C(\epsilon_r - 1)) \\ \epsilon_z = 1 + C(\epsilon_r - 1) \end{cases} \tag{2}$$

and:

$\bar{\bar{\epsilon}}_r$ - is the tensor of the relative dielectric permittivity

ϵ_t - is the transversal relative dielectric permittivity

ϵ_z - is the tangential relative dielectric permittivity

C - is the dielectric concentration given by:

$$C = (A_T - NA_F) / A_T \tag{3}$$

where

A_T – is the transversal area of the dielectric rod

A_F - is the transversal area of the holes (it is assumed that the holes have the same transversal area)

and N - is the hole numbers.

C. Theoretical Formulation

Considering the geometry of the problem shown in Figure 1, in region $r < r_0$, the longitudinal field components E_z and H_z must satisfy the wave equation and the solutions are given by a mode expansion inside and outside the rod.

Inside the dielectric rod ($r < r_1$):

$$Ei_{zn}(r, \phi, z) = K^2 A_n J_n(Kr) \cos(n\phi) e^{-\gamma z} \tag{4}$$

$$Hi_{zn}(r, \phi, z) = y_i K^2 B_n J_n(Kr) \sin(n\phi) e^{-\gamma z} \tag{5}$$

with

$$K^2 = k_0^2 \epsilon_z + \gamma^2 \tag{6}$$

Outside the dielectric rod ($r_1 < r < r_0$):

$$Eo_{zn}(r, \phi, z) = k_1^2 (C_n J_n(k_1 r) + D_n Y_n(k_1 r)) \cos(n\phi) e^{-\gamma z} \tag{7}$$

$$Ho_{zn}(r, \phi, z) = y_o k_1^2 (E_n J_n(k_1 r) + F_n Y_n(k_1 r)) \sin(n\phi) e^{-\gamma z} \tag{8}$$

with

$$k_1^2 = k_0^2 + \gamma^2 \tag{9}$$

and

$y_i = \sqrt{\epsilon_0 / \mu_0} \sqrt{\epsilon_z} = y_o \sqrt{\epsilon_z}$ is the intrinsic dielectric admittance, y_o is the intrinsic air admittance, γ is the propagation constant, with $\gamma = \alpha + j\beta \cong j\beta = \gamma_z$, for the lossless case. k_0 is the free space wave number. $J_n(x)$ and $Y_n(x)$ are Bessel functions of first and second kind of order n , respectively.

The ϕ -component of the fields are given by:

$$Ei_\phi(r, \phi, z) = \left(\frac{n\gamma}{r} A_n J_n(Kr) + j\omega\mu_0 y_i K B_n J'_n(Kr) \right) \sin(n\phi) e^{-\gamma z} \tag{10}$$

$$H_{i_\phi}(r, \phi, z) = - \left(\frac{n\gamma y_i}{r} B_n J_n(Kr) + j\omega \epsilon_0 \epsilon_i K A_n J'_n(Kr) \right) \cos(n\phi) e^{-\gamma z} \tag{11}$$

$$E_{o_\phi}(r, \phi, z) = \left(\frac{n\gamma}{r} (C_n J_n(k_1 r) + D_n Y_n(k_1 r)) + j\omega \mu_0 y_o k_1 (E_n J'_n(k_1 r) + F_n Y'_n(k_1 r)) \right) \sin(n\phi) e^{-\gamma z} \tag{12}$$

$$H_{o_\phi}(r, \phi, z) = - \left(\frac{n\gamma y_o}{r} (E_n J_n(k_1 r) + F_n Y_n(k_1 r)) + j\omega \epsilon_0 k_1 (C_n J'_n(k_1 r) + D_n Y'_n(k_1 r)) \right) \cos(n\phi) e^{-\gamma z} \tag{13}$$

Next, the boundary conditions are applied considering the surface-impedance approach instead of the use of space harmonics. This is a good approximation for slot width smaller than a tenth of a wavelength [2]. The approximation improves as the number of slots per wavelength increases. Application of boundary conditions will produce a system of equations that must be numerically solved to obtain the propagation constant for the hybrid modes HE and EH. The system of equations is presented below:

$$\begin{pmatrix} \alpha_{11} & \alpha_{12} & \alpha_{13} & \alpha_{14} & \alpha_{15} & \alpha_{16} \\ \alpha_{21} & \alpha_{22} & \alpha_{23} & \alpha_{24} & \alpha_{25} & \alpha_{26} \\ \alpha_{31} & \alpha_{32} & \alpha_{33} & \alpha_{34} & \alpha_{35} & \alpha_{36} \\ \alpha_{41} & \alpha_{42} & \alpha_{43} & \alpha_{44} & \alpha_{45} & \alpha_{46} \\ \alpha_{51} & \alpha_{52} & \alpha_{53} & \alpha_{54} & \alpha_{55} & \alpha_{56} \\ \alpha_{61} & \alpha_{62} & \alpha_{63} & \alpha_{64} & \alpha_{65} & \alpha_{66} \end{pmatrix} \begin{pmatrix} A_n \\ B_n \\ C_n \\ D_n \\ E_n \\ F_n \end{pmatrix} = \begin{pmatrix} 0 \\ 0 \\ 0 \\ 0 \\ 0 \\ 0 \end{pmatrix} \tag{14}$$

where:

$$\alpha_{11} = \alpha_{12} = \alpha_{21} = \alpha_{22} = \alpha_{32} = \alpha_{35} = \alpha_{36} = \alpha_{41} = \alpha_{43} = \alpha_{44} = 0 \tag{15}$$

$$\alpha_{13} = \frac{n\gamma}{r_0} J_n(k_1 r_0) \tag{16}$$

$$\alpha_{14} = \frac{n\gamma}{r_0} Y_n(k_1 r_0) \tag{17}$$

$$\alpha_{15} = j\omega \mu_0 k_1 y_o J'_n(k_1 r_0) \tag{18}$$

$$\alpha_{16} = j\omega \mu_0 k_1 y_o Y'_n(k_1 r_0) \tag{19}$$

$$\alpha_{23} = j\omega k_1 \epsilon_0 J'_n(k_1 r_0) + k_1^2 Y_s(r_0) J_n(k_1 r_0) \tag{20}$$

$$\alpha_{24} = j\omega k_1 \epsilon_0 Y'_n(k_1 r_0) + k_1^2 Y_s(r_0) Y_n(k_1 r_0) \tag{21}$$

$$\alpha_{25} = \frac{n\gamma}{r_0} y_o J_n(k_1 r_0) \tag{22}$$

$$\alpha_{26} = \frac{n\gamma}{r_0} y_o Y_n(k_1 r_0) \tag{23}$$

$$\alpha_{31} = K^2 J_n(Kr_1) \tag{24}$$

$$\alpha_{33} = -k_1^2 J_n(k_1 r_1) \tag{25}$$

$$\alpha_{34} = -k_1^2 Y_n(k_1 r_1) \tag{26}$$

$$\alpha_{42} = y_i K^2 J_n(Kr_1) \tag{27}$$

$$\alpha_{45} = -y_o k_1^2 J_n(k_1 r_1) \tag{28}$$

$$\alpha_{46} = -y_o k_1^2 Y_n(k_1 r_1) \tag{29}$$

$$\alpha_{51} = \frac{n\gamma}{r_1} J_n(Kr_1) \tag{30}$$

$$\alpha_{52} = j\omega \mu_0 y_i K J'_n(Kr_1) \tag{31}$$

$$\alpha_{53} = -\frac{n\gamma}{r_1} J_n(k_1 r_1) \tag{32}$$

$$\alpha_{54} = -\frac{n\gamma}{r_1} Y_n(k_1 r_1) \alpha_{52} = j\omega \mu_0 y_i K J'_n(Kr_1) \tag{33}$$

$$\alpha_{55} = -j\omega \mu_0 y_o k_1 J'_n(k_1 r_1) \tag{34}$$

$$\alpha_{56} = -j\omega \mu_0 y_o k_1 Y'_n(k_1 r_1) \tag{35}$$

$$\alpha_{61} = -j\omega \epsilon_0 \epsilon_t K J'_n(Kr_1) \tag{36}$$

$$\alpha_{62} = -\frac{n\gamma}{r_1} y_i J_n(Kr_1) \tag{37}$$

$$\alpha_{63} = j\omega\epsilon_0 k_1 J'_n(k_1 r_1) \tag{38}$$

$$\alpha_{64} = j\omega\epsilon_0 k_1 Y'_n(k_1 r_1) \tag{39}$$

$$\alpha_{65} = \frac{n\gamma}{r_1} y_o J_n(k_1 r_1) \tag{40}$$

$$\alpha_{66} = \frac{n\gamma}{r_1} y_o Y_n(k_1 r_1) \tag{41}$$

and $Y_s(r_0)$ is the surface admittance given by:

$$Y_s(r_0) = -jy_0 \left\{ \frac{J'_n(k_0 r_0) Y_n(k_0 r_2) - J_n(k_0 r_2) Y'_n(k_0 r_0)}{J_n(k_0 r_0) Y_n(k_0 r_2) - J_n(k_0 r_2) Y_n(k_0 r_0)} \right\} \tag{42}$$

The far-fields are obtained by applying the Fourier Transform in the aperture tangential fields [6].

$$E_{\theta rad} = C \int_0^{2\pi} \int_0^{r_0} E_{\theta} e^{jkr' \sin \theta \cos(\phi - \phi')} r' dr' d\phi' \tag{43}$$

$$E_{\phi rad} = C \int_0^{2\pi} \int_0^{r_0} E_{\phi} e^{jkr' \sin \theta \cos(\phi - \phi')} r' dr' d\phi' \tag{44}$$

The co-polar and cross polar fields are obtained by using Ludwig's third definition [7].

III. SIMULATED RESULTS

Some particular cases were simulated to validate the theoretical development presented in this article and to analyze the dielectric rod anisotropy effect in the structure. The particular geometry used has $r_1 = 0.05054\text{m}$, $r_0 = 0.06317\text{m}$ and corrugation depth $d = 0.014\text{m}$. Initially it was considered an isotropic dielectric rod with $\epsilon_r = 1.05$ in order to compare the results with the existing literature [4]. Fig 2 presents the simulated results. As it was expected, the two curves (corrugated [4] and dielectric-corrugated) are very close. The dielectric-corrugated-guide curve for the HE11 mode crosses $(\beta/k_0) = 1$ tending to square root of ϵ_r , but don't pass this value for a wide frequency band. In other simulation, an isotropic dielectric rod with $\epsilon_r = 10.3$ (Alumina Ceramic) [8] is perforated with 450 holes (diameter=4mm). The holes were axial and homogenously distributed in the rod area. As result, it was obtained an equivalent anisotropic material with $\epsilon_z = 3.745$ and $\epsilon_t = 2.737$. The simulated dispersion

curves, for the two main modes, are presented in the Fig 3. In this figure, it is also presented the dispersion curves for the isotropic dielectric rod with $\epsilon_r = 3.745$. The isotropic permittivity value $\epsilon_r = 3.745$ can be obtaining with: “Cross linked poly styrene / ceramic powder-filled, Silicone resin ceramic powder-filled, air with rexolite standoffs fused quartz” [8].

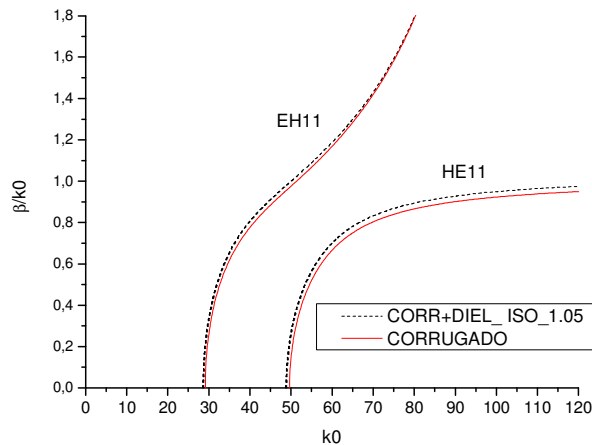


Fig. 2. Simulated dispersion curves for the degenerate case of an isotropic dielectric rod with $\epsilon_r=1.05$, and for the hollow cylindrical corrugated guide [4]. $r_1=0.05054\text{m}$, $r_0=0.06317\text{m}$ and corrugation depth $d=0.014\text{m}$.

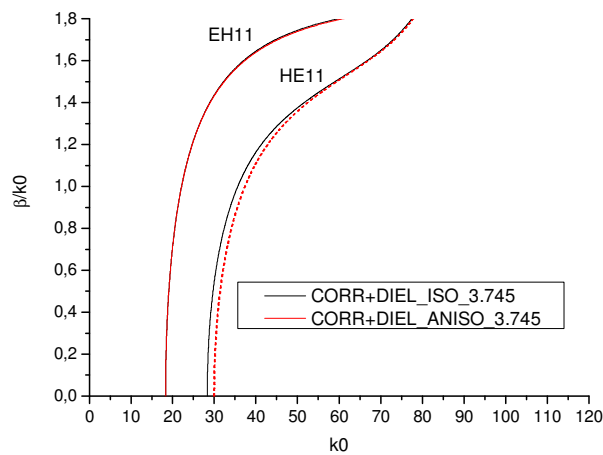


Fig. 3. Simulated dispersion curves. Parameters: $r_1=0.05054\text{m}$, $r_0=0.06317\text{m}$ and corrugated depth $d=0.014\text{m}$. Anisotropy was created by inserting 450 axial holes, with diameter $\phi=4\text{ mm}$, in the dielectric with $\epsilon_r=10.3$ resulting $\epsilon_r=2.737$ and $\epsilon_z=3.745$. Isotropic dielectric $\epsilon_r=3.745$.

The isotropic simulated curves, presented in Fig 3, were compared and agreed with existing literature [2-4]. When dielectric anisotropy is present, the HE11 dispersion curve moves to the right. This result in an elevation of cut-off frequency. The same effect was not observed for the EH11 dispersion curve.

The co- and cross polar radiated far-fields for both cases of Fig 3 (isotropic and anisotropic) are presented in Fig 4. In this simulation it was considered $f=5.252$ GHz ($k_0=110$) and only the presence of the main mode HE11.

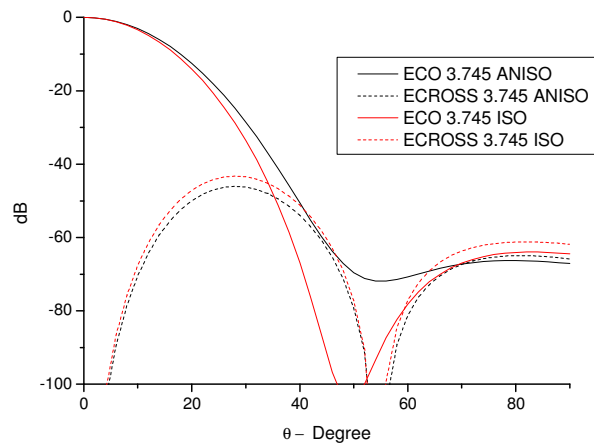


Fig. 4. Co-polar and cross-polar radiated fields for the balanced hybrid HE11-mode. Plane 45° . Parameters: $r_1=0.05054$ m, $r_0=0.06317$ m and corrugation depth $d=0.014$ m. Anisotropy created by 450 holes axial, with diameter $\phi=4$ mm, in the dielectric with $\epsilon_r=10.3$ resulting $\epsilon_r=2.737$ and $\epsilon_z=3.745$. Isotropic dielectric $\epsilon_r=3.745$.

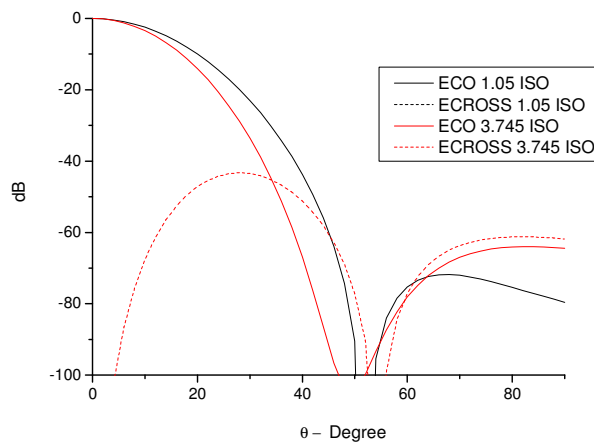


Fig. 5. Co-polar and cross-polar radiated fields. Plane 45° . Parameters: $r_1=0.05054$ m, $r_0=0.06317$ m and corrugated depth $d=0.014$ m. Isotropic dielectric $\epsilon_r=3.745$ and isotropic dielectric $\epsilon_r=1.05$.

In the Fig 5 are showed the co- and cross polar radiation curves for the isotropic cases of $\epsilon_r = 1.05$ and $\epsilon_r = 3.745$ for the same frequency utilized in the figure 4. In this figure, it is observed cross polarization levels low than -100 dB for the isotropic case $\epsilon_r=1.05$.

IV. CONCLUSIONS

This paper presented the characteristic equation developed for the corrugated cylindrical guide with anisotropic dielectric rod. The hybrid modes dispersion curves generated by this characteristic equation were tested with the degenerated case of a hollow cylindrical corrugated guide by using an isotropic dielectric with: $\epsilon_r = 1.05$. The results were presented in the Figure 2 and showed very close agreement. This was expected, since the dielectric was very close to unity. In this case the structure is almost the same the structure of the corrugated guide. This paper also presented and compared simulated dispersion curves for the degenerated case of isotropic dielectric with $\epsilon_r = 3.745$ and the case of an anisotropic dielectric with $\epsilon_z = 3.745$ and $\epsilon_t = 2.737$. This anisotropic material was created by perforating an isotropic material with $\epsilon_r = 10.3$ according to the technique describe in this article. In both cases the dispersion curves were identical for the mode EH11 and little difference were observed for the mode HE11. The anisotropic HE11 mode presented cut-off value higher than isotropic one. This is because of the smaller permittivity in the transversal direction. The radiation pattern of Figure 4 shows that the anisotropy effect created an increment of approximately 3dB in the cross polarization level. The co-polar radiated field presented lower level second lobe for the anisotropic case. This effect is very interesting and demands more study for its understanding. From the curves presented in Figure 5, it can be verified that the cross polarization were significantly worse with the highest permittivity isotropic dielectric inclusion. It is predictable, because the structure with $\epsilon_r = 1.05$ is an structure similar to the hollow cylindrical corrugated guide with corrugation depth $d = \lambda/4$, for this case excellent levels of cross polarization are expected. This paper also presented a technique to reduce the relative permittivity and generate uniaxial anisotropy from an homogeneous isotropic dielectric. The objective is to obtain a material more homogeneous and mechanic-structurally better than the dielectric foam. The anisotropy created by this technique showed little effect in the dispersion curves and radiation patterns simulated examples. More detailed studies are being carried out to improve the conclusions on the anisotropic effect in the proposed guide.

ACKNOWLEDGMENT

The authors would like to acknowledge the Brazilian agencies: CNPq and CAPES-PROCAD.

REFERENCES

- [1] P.D.Potter, "A new horn antenna with suppressed sidelobes and equal beamwidth," *Microwave J.*, pp. 71–78, June 1963.
- [2] P. J. B. Clarricoats and A. D. Olver, *Corrugated Horns for Microwave Antennas*, London: Peter Peregrinus Ltd, IEE, 1984.
- [3] A. D. Olver, P. J. B. Clarricoats and L. Shafai, *Microwave Horns and Feeds*, London: IEEE Press, Inc., New York, 1994.
- [4] P.J.Clarricoats, J.R.Descardecı and A.D.Olver, "A Low Crosspolar Feed for Broadband Application," 1988-*URSI-International Symp. On Electromagnetic Theory*, Thessaloniki USRI, 1988, v.1. pp. 110-119.
- [5] A.V.Ghiner and G.I.Surdutovich, "Method of Integral Equations and an Extinction Theorem for Two-Dimensional Problems in Nonlinear Optics," *Physical Review A*, vol 50, N.1, July 1994, pp.714-723.
- [6] C.A.Balanis, *Advantage Engineering Electromagnetic*, USA, John Wiley & Sons, 1989.
- [7] A.C.Ludwig, "The Definition of Cross Polarization," *IEEE Transactions on Antennas and Propagation*, January, 1973.

- [8] K.R.Carver, J.W.Mink, "Microstrip Antenna Technology," IEEE Transactions on Antennas and Propagation, vol. 29, No. 1, January, 1981.